The Astrophysical Journal, 587:649–659, 2003 April 20

MOLECULAR GAS IN CANDIDATE DOUBLE-BARRED GALAXIES. II. COOLER, LESS DENSE GAS ASSOCIATED WITH STRONGER CENTRAL CONCENTRATIONS

Glen R. Petitpas
University of Maryland, College Park, MD 20742; petitpas@astro.umd.edu

and

Christine D. Wilson
McMaster University, 1280 Main Street West, Hamilton, ON L8S 4M1, Canada; wilson@physics.mcmaster.ca
Received 2002 June 27; accepted 2003 January 1

ABSTRACT

We have performed a multitransition CO study of the centers of seven double-barred galaxies that exhibit a variety of molecular gas morphologies to determine if the molecular gas properties are correlated with the nuclear morphology and star-forming activity. Near-infrared galaxy surveys have revealed the existence of nuclear stellar bars in a large number of barred or lenticular galaxies. High-resolution CO maps of these galaxies exhibit a wide range of morphologies. Recent simulations of double-barred galaxies suggest that variations in the gas properties may allow it to respond differently to similar gravitational potentials. We find that the ^{12}CO $J = 3$–$2/J = 2$–1 line ratio is lower in galaxies with centrally concentrated gas distributions and higher in galaxies with CO emission dispersed around the galactic center in rings and peaks. The ^{13}CO/^{12}CO $J = 2$–1 line ratios are similar for all galaxies, which indicates that the $J = 3$–$2/J = 2$–1 line ratio is tracing variations in gas temperature and density, rather than variations in optical depth. There is evidence that the galaxies which contain more centralized CO distributions are composed of molecular gas that is cooler and less dense. Observations suggest that the star formation rates are higher in the galaxies containing the warmer, denser, less centrally concentrated gas. It is possible that either the bar dynamics are responsible for the variety of gas distributions and densities (and hence the star formation rates) or that the star formation alone is responsible for modifying the gas properties.

Subject headings: galaxies: active — galaxies: ISM — galaxies: nuclei — galaxies: starburst

1. INTRODUCTION

Recent near-infrared (NIR) surveys reveal isophote twists in the central regions of barred galaxies, which are thought to be the signature of a bar within a bar (e.g., Mulchaey, Regan, & Kundu 1997). Recent models of double-barred galaxies have had some success in reproducing relatively long-lived central features that can explain the isophote twists. Shaw et al. (1993) model galaxies as gravitational stars and dissipative gas clouds and find that the NIR isophote twists are caused by viscous and gravitational torques that drag the central regions of the main bar out of alignment with the rest of the bar. Friedli & Martinet (1993) suggest that the NIR isophote twists are the result of a kinematically distinct "nuclear bar" that can rotate with up to 6 times the pattern speed of the large-scale bar. One thing these models have in common is the need for dissipation. Both groups have to include large amounts of molecular gas in order for the models to be able to reproduce and sustain the observed features. The models of barred galaxies by Combes & Gerin (1985), Shaw et al. (1993), and Friedli & Martinet (1993) produce very different nuclear morphologies by varying the amount of gaseous component included in the simulations. More problematically, the models of Combes (1994) and Maciejewski et al. (2002) exhibit different central morphologies by simply changing the *properties* of the interstellar medium.

In an attempt to test these models, we have undertaken a study of the molecular gas properties of a sample of galaxies believed to contain double bars based on the NIR isophote twists observed in their nuclei (see Tables 1 and 2). In Paper I (Petitpas & Wilson 2002) we find that, despite similarities in the NIR images, the CO maps show very different morphologies. For example, the CO maps of NGC 2273, NGC 2782, and NGC 4736 exhibit what may be interpreted as nuclear bars that align with the nuclear NIR isophote twists (Petitpas & Wilson 2002; Jogee, Kenney, & Smith 1999; Wong & Blitz 2000), while NGC 6951 shows twin peaks of molecular gas collecting at an inner Lindblad resonance (ILR; Kohno, Kawabe, & Vila-Vilaró 1999). NGC 5728 shows a very disordered CO structure, where the clumps of CO emission do not seem to align with any structures seen at other wavelengths (Petitpas & Wilson 2002).

Simulations of galaxies (both single- and double-barred) have shown that the details of the nuclear structure and inflow rates depend on the assumed gas properties of the models. For example, Combes (1994) demonstrated that the nuclear bar of a double-barred galaxy can either be phase-locked (as predicted by Shaw et al. 1993) or kinematically separated from the primary bar (as predicted by Friedli & Martinet 1993), depending on the gas viscosity in the models. More recently, Maciejewski et al. (2002) modeled the flow of gas in a realistic double-barred potential and found that the inflow rates depend on the sound speed of the interstellar medium. Galaxies with high sound speeds had greater inflow rates, and the gas was able to reach all the way into the nucleus. In the galaxies with lower sound speeds, the infalling gas is trapped into a circumnuclear ring near the ILR, and even the torques exerted by the nuclear stellar bar are not enough to transport the gas inward beyond the ring. This model suggests that nuclear bars may not be an effective means of fueling active galactic nuclei

TABLE 1
GALAXY PROPERTIES

Galaxy	R.A. (J2000)	Decl. (J2000)	V_{LSR} (km s^{-1})	d (Mpc)	RC3 Classification	Nuclear Activity
NGC 0470.....	01 19 44.8	+03 24 35	2374	32	SA(rs)b	Starburst
NGC 1097.....	02 46 19.0	−30 16 29	1275	17	(R′$_1$)SB(r′l)b	Seyfert 1
NGC 2273.....	06 50 08.7	+60 50 45	1871	25	SB(r)a	Seyfert 2
NGC 3081.....	09 59 29.5	−22 49 35	2385	32	(R$_1$)SAB(r)0/a	Seyfert 2
NGC 4736.....	12 50 53.0	+41 07 14	308	4	(R)SA(r)ab	LINER
NGC 5728.....	14 42 23.9	−17 15 10	2788	37	(R$_1$)SAB(r)a	Seyfert 2
NGC 6951.....	20 37 14.5	+66 06 20	1424	19	SAB(rs)bc	Seyfert 2

NOTES.—Units of right ascension are hours, minutes, and seconds, and units of declination are degrees, arcminutes, and arcseconds. All data taken from the NASA IPAC Extragalactic Database. Distances are derived assuming $H_0 = 75$ km s^{-1} kpc^{-1}.

(AGNs) as originally proposed by Shlosman, Frank, & Begelman (1989).

While the current generation of millimeter and submillimeter telescopes are not capable of resolving molecular gas on the parsec scales needed to resolve the AGN fueling mechanisms directly, we can study the gas within the regions of the ILR. In this paper we present a detailed set of molecular gas data for a sample of double-barred galaxies. We have chosen seven galaxies that are known to contain nuclear stellar bars based on their NIR images (see, e.g., Shaw et al. 1993; Friedli et al. 1996; Jungwiert, Combes, & Axon 1997; Mulchaey et al. 1997; Wozniak et al. 1995), of which five have high-resolution ^{12}CO $J = 1$–0 data published. The properties of these galaxies are summarized in Table 1. This sample will allow us to determine if variations in molecular gas properties are linked in some way to the wide variety of CO morphologies in a sample of galaxies with similar NIR morphologies, as hinted at by the models of Combes (1994) and Maciejewski et al. (2002).

In § 2 we discuss the observations and data reduction techniques. In § 3 we determine the molecular gas physical condition using the local thermodynamic equilibrium (LTE) and large velocity gradient (LVG) approximations. In § 4 we discuss observed correlations between our CO line ratios with the high-resolution CO morphology and simulations of double-barred galaxies. In § 5 we speculate on possible origins of the observed correlations. This work is summarized in § 6.

TABLE 2
PRIMARY AND SECONDARY BAR PROPERTIES

Galaxy	L_1 (kpc)	ϵ_1	L_2 (kpc)	ϵ_2	Reference
NGC 0470.....	4.6	0.55	1.2	0.42–0.46	1, 2
NGC 1097.....	6.6	0.67	0.9	0.42–0.46	1, 2
NGC 2273.....	2.9	0.37	1.0	0.28	3
NGC 3081.....	6.0	0.65–0.66	1.6	0.37–0.42	1, 2
NGC 4736.....	...	...	0.6	∼0.3	4
NGC 5728.....	13.2	0.71	0.8	0.49	1
NGC 6951.....	4.5	0.5–0.6	0.5	0.31	1, 2

NOTES.—L_1 and L_2 are the lengths of the primary and secondary bars, respectively, while ϵ_1 and ϵ_2 are the ellipticities of the primary and secondary bars, respectively. Physical sizes are derived assuming $H_0 = 75$ km s^{-1} kpc^{-1}.

REFERENCES.—(1) Wozniak et al. 1995; (2) Friedli et al. 1996; (3) Mulchaey et al. 1997; (4) Moellenhoff, Matthias, & Gerhard 1995.

2. OBSERVATIONS AND DATA REDUCTION

The nuclei of seven double-barred galaxies were observed using the James Clerk Maxwell Telescope (JCMT)[1] over the period of 1998–2001. We have obtained ^{12}CO $J = 2$–1, ^{13}CO $J = 2$–1, and ^{12}CO $J = 3$–2 detections for all galaxies listed in Table 1 except ^{13}CO $J = 2$–1 in NGC 3081. The half-power beam width of the JCMT is 21″ at 230 GHz (^{12}CO $J = 2$–1) and 14″ at 345 GHz (^{12}CO $J = 3$–2). ^{12}CO $J = 3$–2 data were obtained on a five-point cross offset by 7″ in order to allow convolution to match the 21″ beam of the JCMT at 230/220 GHz. All observations were obtained using the Digital Autocorrelation Spectrometer in beam-switching mode with a 180″ throw. The calibration was monitored by frequently observing spectral line calibrators. The spectral line calibrators showed very little scatter from the published values with individual measurements differing by typically less than 15% from standard spectra. Thus, we adopt the nominal main-beam efficiencies (η_{MB}) from the JCMT Users Guide of 0.69 at 230/220 GHz and 0.63 at 345 GHz.

Initially, similar data sets were averaged together using the software package SPECX. Spectra were output to FITS files, and then the data were further reduced using the Bell Labs data reduction package COMB. The data were binned to 10 km s^{-1} resolution (7.8 and 11.5 MHz at 230 and 345 GHz, respectively), and zeroth- or first-order baselines were removed. The emitting regions were quite wide (>200 km s^{-1}), but the spectrometer bandwidth was at least 800 km s^{-1}, which allowed for accurate baseline determination. Finally, the five ^{12}CO $J = 3$–2 spectra for each galaxy were convolved to simulate a 21″ beam. The spectra for each galaxy are shown in Figure 1, and the spectral line intensities are summarized in Table 3.

The data were then binned to 20 km s^{-1} resolution. This allowed the calculation of line ratios for each channel within the spectral line. The ratios for each channel were averaged using equal weights to obtain the final line ratios. Only those channels with a signal-to-noise ratio (S/N) of at least 2 in the line ratio were used in the calculation. The uncertainty in the line ratio is taken as the standard deviation of the

[1] The JCMT is operated by the Joint Astronomy Centre in Hilo, Hawaii, on behalf of the parent organizations Particle Physics and Astronomy Research Council in the United Kingdom, the National Research Council of Canada, and The Netherlands Organization for Scientific Research.

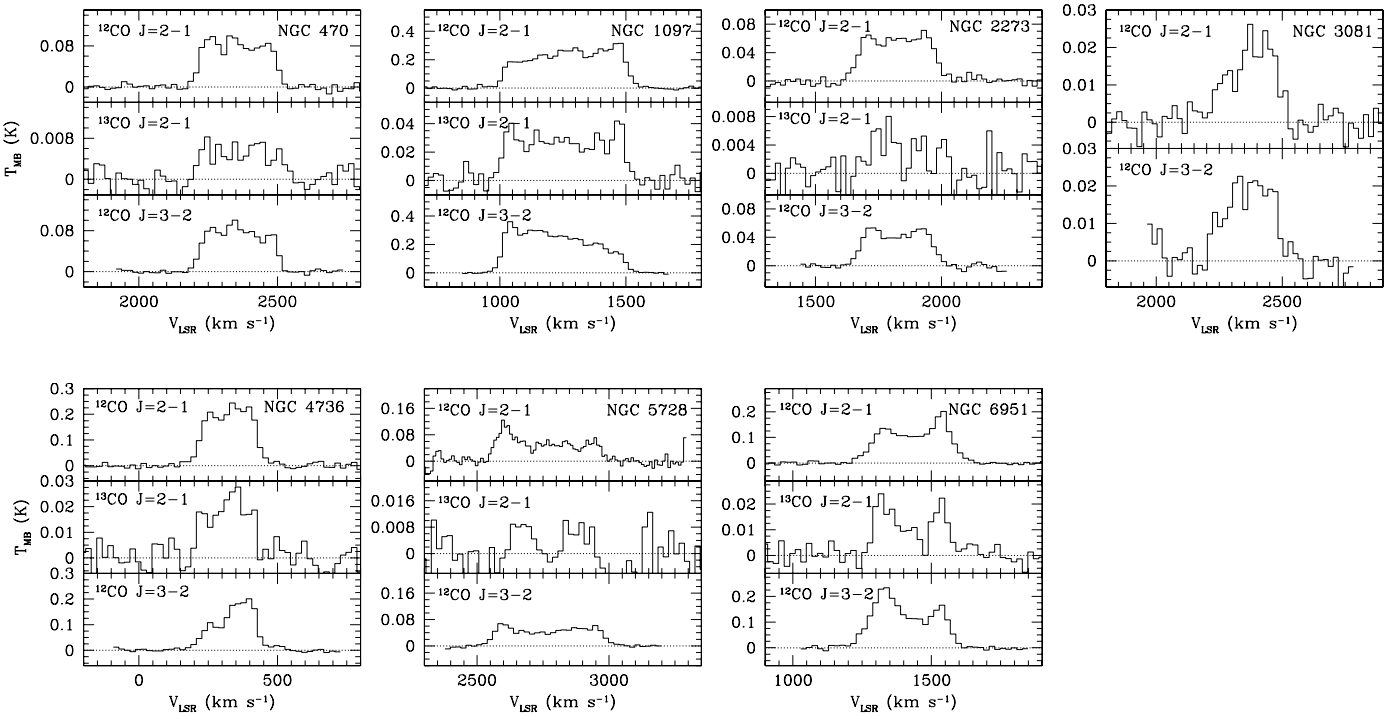

FIG. 1.—Individual spectra for the inner 21″ of each galaxy. The top panel shows ^{12}CO $J = 2$–1, the middle panel shows ^{13}CO $J = 2$–1, and the bottom panel shows ^{12}CO $J = 3$–2 (convolved to 21″ resolution). The vertical scales for the ^{12}CO $J = 2$–1 and ^{12}CO $J = 3$–2 spectra are the same, while the scale of the ^{13}CO $J = 2$–1 spectra is 10 times smaller for each galaxy.

mean. As a final step, the spectra and line ratios were scaled to the main-beam temperature scale using the appropriate values for $\eta_{\rm MB}$ (see above). A summary of the line ratios is given in Table 4, and channel-by-channel histograms of the ratios are shown in Figure 2.

The channel-by-channel ^{12}CO $J = 3$–$2/J = 2$–1 line ratios for NGC 1097 and NGC 6951 shown in Figure 2 show evidence for gradients. This may be caused by pointing offsets in the observations of one transition relative to the other, or it may reflect a true gradient in excitation temperature across the nuclei of these galaxies. The individual line profiles for the central positions are similar in the ^{12}CO $J = 3$–2 and ^{12}CO $J = 2$–1 data for these galaxies, suggesting that large pointing offsets are not present. Evidence for similar gradients has been seen in the nearby starburst galaxy M82 (Petitpas & Wilson 2000) and may be caused by variation in star formation strengths across the nuclei. In the case of NGC 1097, the slight gradient could easily be produced by slight pointing offsets, but the gradient in NGC 6951 is strong enough that it may reflect true variations in excitation temperature across the nucleus of this galaxy. In either case, we are averaging the gas properties across the entire nucleus, so the gradients (real or artificial) will not significantly affect our results.

For § 3.2, the LVG models contain four free parameters, so we need more line ratios in order to place stronger

TABLE 3
SPECTRAL LINE PARAMETERS

Galaxy	^{12}CO $J = 2$–1[a]	^{13}CO $J = 2$–1[a]	^{12}CO $J = 3$–2[a]	^{12}CO $J = 3$–2[b]	^{12}CO $J = 1$–0	Reference
NGC 0470.....	24.2 ± 0.5	1.8 ± 0.2	22.4 ± 0.3	24.9 ± 0.6	19.3[b]	1
NGC 1097.....	121 ± 1	14.6 ± 0.6	121.7 ± 0.5	137.5 ± 0.8	80[b]	2
NGC 2273.....	19.7 ± 0.5	1.2 ± 0.2	14.3 ± 0.3	17.9 ± 0.5	22.5[c]	3
NGC 3081.....	4.6 ± 0.3	...	4.9 ± 0.3	7.4 ± 0.5	...	...
NGC 4736.....	46.1 ± 0.8	4.6 ± 0.4	31.9 ± 0.4	32.9 ± 0.5	32.5[b]	4
NGC 5728.....	24.6 ± 0.6	(0.8 ± 0.8)	21.5 ± 0.4	26.5 ± 0.8	9.74[b]	2
NGC 6951.....	41.7 ± 0.6	4.2 ± 0.4	48.8 ± 0.5	59.4 ± 0.8	71[b]	5

NOTES.—All CO line strengths are in K km s^{-1} in $T_{\rm MB}$. The beam sizes for the first four columns are stated below the transition. The ^{12}CO $J = 1$–0 beam sizes are given beside the flux value. Observations of ^{13}CO $J = 2$–1 in NGC 3081 were not attempted.

[a] 21″ resolution.

[b] 16″ resolution.

[c] 22″ resolution.

REFERENCES.—(1) Sofue et al. 1993; (2) Vila-Vilaró, Taniguchi, & Nakai 1998; (3) Kruegel, Chini, & Steppe 1990; (4) Shioya et al. 1998; (5) Kohno et al. 1999.

TABLE 4
CO Line Ratios and Nuclear Characteristics

Galaxy	$\frac{^{13}CO\ J=2-1}{^{12}CO\ J=2-1}$[a]	$\frac{^{12}CO\ J=3-2}{^{12}CO\ J=2-1}$[a]	$\frac{^{12}CO\ J=2-1}{^{12}CO\ J=1-0}$[b]	Nuclear CO	Activity[c]	Reference
NGC 0470.....	0.09 ± 0.01	0.93 ± 0.03	1.38 ± 0.42	Elongated	SB	1, 2
NGC 1097.....	0.13 ± 0.01	1.03 ± 0.07	1.67 ± 0.50	Ring?	S1	3, 4
NGC 2273.....	0.11 ± 0.01	0.75 ± 0.05	0.88 ± 0.26	Elongated	S2	3, 5, 6
NGC 3081.....	...	1.2 ± 0.2	...	?	S2	7
NGC 4736.....	0.10 ± 0.01	0.67 ± 0.04	0.70 ± 0.14	Bar/peak	L	8, 9
NGC 5728.....	<0.09	1.01 ± 0.06	1.96 ± 0.59	Irregular	S2	3, 6
NGC 6951.....	0.13 ± 0.02	1.4 ± 0.2	0.59 ± 0.18	Twin peaks	S2	3, 10, 11

[a] All data for these columns are taken with the JCMT. The line ratio calculation is described in the text.

[b] The $^{12}CO\ J = 1–0$ data for NGC 2273 is taken with the IRAM 30 m telescope with a 22″ beam. The line ratio for NGC 4736 is taken from Gerin et al. 1991 with a 22″ beam. The remaining ratios are a combination of $^{12}CO\ J = 3–2$ data taken with the JCMT (16″ beam) and $^{12}CO\ J = 1–0$ data taken with the Nobeyama 45 m telescope (16″ beam). The $^{12}CO\ J = 3–2/J = 1–0$ ratio is scaled to the $^{12}CO\ J = 2–1/J = 1–0$ ratio by dividing by the $^{12}CO\ J = 3–2/J = 2–1$ ratio in col. (3). All ratios are given in T_{MB}.

[c] SB = Starburst; S1 = Seyfert 1; S2 = Seyfert 2; L = LINER

References.—(1) Sofue et al. 1993; (2) Jogee 1998; (3) Vila-Vilaró et al. 1998; (4) Gerin et al. 1988; (5) Kruegel et al. 1990; (6) Petitpas & Wilson 2002; (7) Phillips, Charles, & Baldwin 1983; (8) Gerin et al. 1991; (9) Sakamoto et al. 1999; (10) Aalto et al. 1995; (11) Kenney et al. 1992.

constraints on the molecular gas physical conditions. We have searched the literature and have obtained $^{12}CO\ J = 1–0$ line strengths for all galaxies except NGC 3081. All $^{12}CO\ J = 1–0$ spectra were taken with the Nobeyama Radio Observatory (NRO) with 16″ resolution except for NGC 2273, which was taken at the IRAM 30 m telescope with a 22″ beam (see Table 3 for references). Since our JCMT $^{12}CO\ J = 2–1$ data are taken at 21″ resolution, we have created beam-matched $^{12}CO\ J = 3–2/J = 1–0$ ratios with the JCMT and NRO data and divided them by our beam-matched $^{12}CO\ J = 3–2/J = 2–1$ ratio. In the case of NGC 4736, we used the $^{12}CO\ J = 2–1/J = 1–0$ line ratio taken at IRAM with a 22″ beam by Gerin, Casoli, & Combes (1991, since they did not publish the individual line strengths). For the line ratios we took from the literature or created using JCMT and published data, we adopt a 30% uncertainty to account for cross-calibration uncertainties.

3. MOLECULAR GAS PHYSICAL CONDITIONS

All of these galaxies were initially chosen because the NIR images suggested the presence of a nuclear stellar bar.

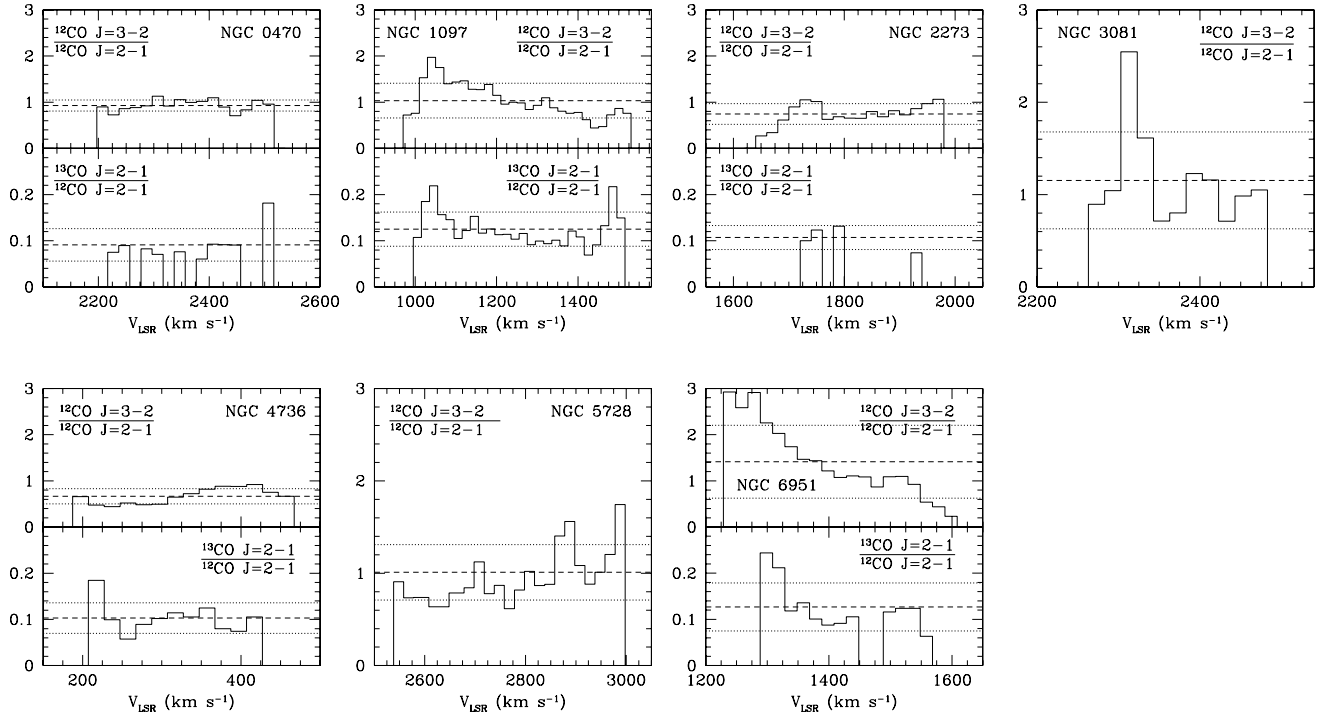

Fig. 2.—Channel by channel line ratios for each galaxy. The top panel shows the $^{13}CO/^{12}CO\ J = 2–1$ ratio, and the bottom panel shows the $^{12}CO\ J = 3–2/J = 2–1$ ratio. Only those channels with a combined S/N less than 2 are shown. The dashed line is the average over all channels; the dotted line is the rms of the scatter. The values for the ratios listed in Table 4 are the average value over all channels shows here, and the uncertainty is the standard deviation in the mean. For all galaxies, the vertical scale ranges 0–3 for the $^{12}CO\ J = 3–2/J = 2–1$ line ratio and 0–0.3 for the $^{13}CO/^{12}CO\ J = 2–1$ line ratio.

The similarities in the NIR images suggest that the gravitational potentials are similar in these galaxies (see Table 2). Models of double-barred galaxies indicate that the gas may behave differently within similar potentials if the gas properties are varied. In this section, we model the CO line ratios to determine the true physical conditions of the molecular gas, such as excitation temperature, kinetic temperature, density, and column density.

Determining the physical conditions of molecular clouds in other galaxies can be very difficult. For single-dish observations, the beam size is usually larger than the angular diameter of typical molecular clouds, and so the line strengths are beam-diluted. In addition, molecular clouds are known to be very clumpy (e.g., Stutzki & Güsten 1990) and the high-resolution ^{12}CO $J = 1$–0 maps of the galaxies in our sample show a variety of distributions within the inner 21″ (Kenney et al. 1992; Jogee 1998; Petitpas & Wilson 2002; Sakamoto et al. 1999), so the average emission likely originates in a mixture of high- and low-density material with different beam-filling factors. For extragalactic sources, the filling factor of the CO emission within the primary beam may be small and is difficult to determine accurately. Thus, for low-resolution, single-dish studies such as this one, it is preferable to study the ratios of line strength, rather than the individual fluxes. As long as the two CO transitions are observed with the same size primary beam, the division of the two eliminates the unknown filling factor of the emission within the beam of the telescope (assuming the two frequencies originate from the same region, which is likely true for these distant sources).

The high-resolution CO maps of these galaxies suggest that most of the emission originates from the regions at or interior to the ILR (as traced by star-forming rings or the ends of nuclear bars). The exception is NGC 4736 for which at 4 Mpc the 21″ primary beam of the JCMT does not cover the entire ILR region (see Wong & Blitz 2000; Fig. 5). In all galaxies, however, the JCMT beam entirely covers the strongest emission regions, which suggests that the physical conditions determined here represent a good approximation of the *average* gas properties within the ILR regions.

In § 3.1 we analyze the line ratios under the LTE approximation. In this model (in addition to the unknown filling factor, f_ν), assumptions have to be made about the optical depth of the emission lines. In § 3.2 we analyze the line ratios under the LVG assumption, which is more complicated but does not require any assumption regarding optical depths.

Calibration differences between different telescopes can introduce (often large) uncertainties in spectral line ratios (see discussion in Tilanus et al. 1991, for example). To prevent the introduction of such uncertainties, we limit our analysis in § 3.1 to the interpretation of only those CO line ratios taken with the JCMT, namely, ^{13}CO/^{12}CO $J = 2$–1 and ^{12}CO $J = 3$–2/$J = 2$–1. In the LVG approximation, we need more than two CO line ratios to place strong constraints on the molecular gas conditions, so in § 3.2 we use all of the line ratios listed in Table 4.

3.1. *LTE Analysis*

In the LTE approximation, we assume that the gas is collisionally dominated, and hence the relative populations between molecular energy levels are a function of a single temperature. There are generally three basic limits with which we are concerned:

1. Both lines are optically thick ($\tau \gg 1$), in which case the integrated intensity line ratio (e.g., ^{12}CO $J = 3$–2/$J = 2$–1) can be written as

$$R_{32/21}^{\rm thick} = \frac{[J_{\nu_{32}}(T_{32}) - J_{\nu_{32}}(T_{\rm bg})]}{[J_{\nu_{21}}(T_{21}) - J_{\nu_{21}}(T_{\rm bg})]} , \quad (1)$$

where $J_\nu(T)$ is proportional to the Planck function (see Kutner & Ulich 1981) and $T_{\rm bg} = 2.7$ K. In LTE ($T_{32} = T_{21} = T_{\rm ex}$) $R_{32/21} \approx 1$ for $T > 30$ K (see Fig. 3).

2. Both lines are optically thin ($\tau \ll 1$), and the integrated intensity line ratio can be written as

$$R_{32/21}^{\rm thin} = \frac{[J_{\nu_{32}}(T_{32}) - J_{\nu_{32}}(T_{\rm bg})]\tau_{32}}{[J_{\nu_{21}}(T_{21}) - J_{\nu_{21}}(T_{\rm bg})]\tau_{21}} , \quad (2)$$

which in LTE depends on the optical depth at each frequency, τ_ν. The ratio of τ-values can be expressed as a function of J, ν, CO-specific constants, and the Boltzmann equation (see, e.g., Scheffler & Elsaesser 1987).

3. One line is optically thick and the other is optically thin, as is likely the case when we compare integrated intensity line ratios for different isotopomers of CO in the same J transition (e.g., ^{13}CO/^{12}CO $J = 2$–1). If we assume $T_{\rm ex}^{\rm 13CO} = T_{\rm ex}^{\rm 12CO}$ and that ^{12}CO $J = 2$–1 is optically thick and ^{13}CO $J = 2$–1 is optically thin, we have

$$R_{12/13} \approx \frac{X}{\tau(^{12}{\rm CO})} , \quad (3)$$

where X is the ^{12}CO/^{13}CO abundance ratio (which is measured to be 43–62 in the Milky Way; Hawkins & Jura 1987; Langer & Penzias 1993).

Plots of the integrated intensity line ratio as a function of excitation temperature for the optically thick and thin cases are given in Figure 3. The excitation temperatures derived from the ^{12}CO $J = 3$–2/$J = 2$–1 line ratio under the assumption of LTE are summarized in Table 5.

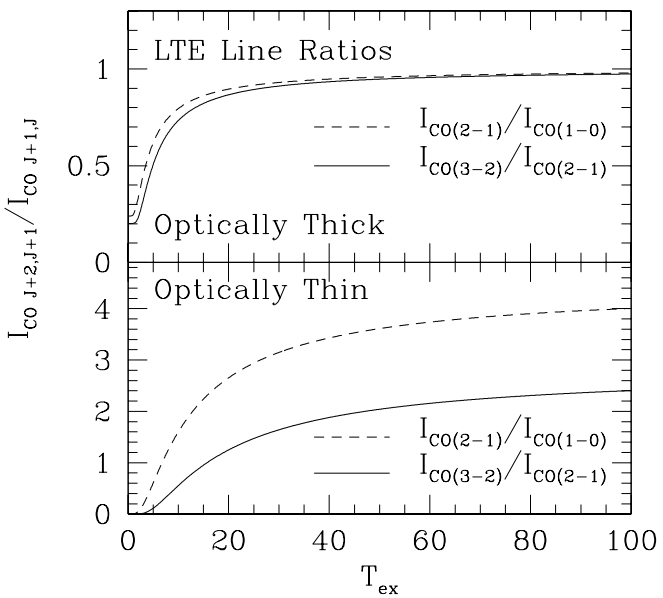

FIG. 3.—Plots of ^{12}CO integrated intensity line ratio as a function of excitation temperature in the LTE approximation.

TABLE 5
LTE Parameters and Dust Temperatures

Galaxy	$T_{ex}^{J=3-2}$ (thin) (K)	$T_{ex}^{J=3-2}$ (thick) (K)	τ_{21}	f_{60}/f_{100}	T_{dust} ($\beta = 2,\ 1$) (K)	Reference
NGC 0470.....	15	>38	3.9	0.51	30, 37	1
NGC 1097.....	16	>66	5.6	0.52	30, 36	1
NGC 2273.....	12	11	4.7	0.60	31, 38	1
NGC 3081.....	18	>150	...	...	...	
NGC 4736.....	11	8	4.2	0.57	31, 37	2
NGC 5728.....	16	>53	<3.9	0.60	31, 38	2
NGC 6951.....	24	...	5.6	0.35	26, 31	1

Notes.—For the optically thick column, we assumed the $-1\ \sigma$ limit for line ratios that were consistent with 1. The missing entries indicated that the line ratios were not consistent with optically thick emission within the uncertainties. For τ we assume a $^{12}CO/^{13}CO$ abundance ratio of 43 (Hawkins & Jura 1987). For T_{dust} the two values represent a dust emissivity (β) of 2 or 1, respectively (Devereux & Young 1990).

References.—(1) Moshir et al. 1990; (2) Soifer et al. 1989.

The $^{12}CO/^{13}CO$ $J = 2$–1 line ratio is uniform at the 2 σ level over all galaxies and has an average value of 0.11. Assuming optically thick ^{12}CO and optically thin ^{13}CO emission, the $^{13}CO/^{12}CO$ $J = 2$–1 line ratio suggests that the ^{12}CO optical depth in all six galaxies is consistent with $\tau \approx 5$. This indicates that the molecular gas is on the border between optically thin and optically thick in all of our galaxies.

In the LTE approximation, we are unable to determine densities accurately, but we can say that, given the similarities in optical depth between the galaxies, the higher ^{12}CO $J = 3$–$2/J = 2$–1 line ratios indicate warmer gas. We discuss the implications of this in later sections.

3.2. *LVG Analysis*

As a doublecheck of the LTE analysis, we have performed a LVG analysis using a code written by Lee Mundy and implemented as part of the MIRIAD data reduction package. A sample of the output from the models is shown in Figure 4. The integrated intensity line ratios are shown as bands that indicate the $\pm 30\%$ upper and lower limits of the line ratios. We adopt 30% to account for the uncertainties involved in spectral line calibration and baseline removal as well as, in the case of the ^{12}CO $J = 2$–$1/J = 1$–0 line ratio, the uncertainties involved in combining spectral lines from different telescopes. Solutions are indicated by the locations where the regions of the different ratio boundaries overlap. In a few cases, only one of the line ratio contours is visible on the plot, so arrows indicate the allowed region. A gray-scale representation of the ^{12}CO $J = 3$–$2/J = 2$–1 line ratio is included to aid interpretation of this figure. A single component model provided an adequate fit to the observed line ratios in most cases.

There are four main variables in the LVG models: CO column density per unit velocity [$N(CO)/dv$], molecular hydrogen density [$n(H_2)$], kinetic temperature (T_{kin}), and the $^{12}CO/^{13}CO$ abundance ratio ([^{12}CO]/[^{13}CO]). With only three line ratios, we cannot place very strong constraints on the physical conditions of the molecular gas. We have performed a study of parameter space ranging from $15 < \log N(CO)/dv(cm^{-2}/km\ s^{-1}) < 21$, $1 < \log n(H_2)(cm^{-3}) < 6$, $30 < [^{12}CO]/[^{13}CO] < 70$, and $30\ K < T_{kin} < 100\ K$. In general, solutions were found for all temperatures and abundance ratios. Changes in the [^{12}CO]/[^{13}CO] ratio made negligible changes to the solution compared to changes in the kinetic temperature. For this reason, we adopt [^{12}CO]/[^{13}CO] = 50, consistent with the value obtained for the Milky Way (Hawkins & Jura 1987; Langer & Penzias 1993). The derived values from the LVG analysis are summarized in Table 6. For the purpose of clarity, we show results only for $T_{kin} = 30$ K (consistent with the dust temperatures determined by the *IRAS* fluxes; see Table 5).

In many cases we can only determine lower limits to the molecular hydrogen density, and thus we have upper limits on the optical depth. It is interesting that all galaxies have rather similar column densities of CO per unit velocity (within the uncertainty). They are generally all $\sim 10^{17}$ cm^{-2} (km s^{-1})$^{-1}$. If we wish to convert this to a true column

TABLE 6
LVG Solutions for a Kinetic Temperature of 30 K

Galaxy	$\log N(CO)/dv$	$\log n(H_2)$	τ_{10}	τ_{21}	τ_{32}
NGC 0470.....	16.8 ± 0.3	>3.7	<1.6	<5.4	<7.4
NGC 1097.....	17.0 ± 0.1	>4.5	<2.3	<7.2	<10
NGC 2273.....	18.0 ± 1.1	Unbounded	<64	<190	<190
NGC 4736.....	17.0 ± 0.1	3.1 ± 0.3	4.9	14	19
NGC 5728.....	<16.5	>4.1	<0.5	<2.1	<2.9
NGC 6951[a]	<16.5	>4.6	<0.5	<1.9	<2.7

[a] Constraints are based only on the ^{12}CO $J = 3$–$2/J = 2$–1 line ratio.

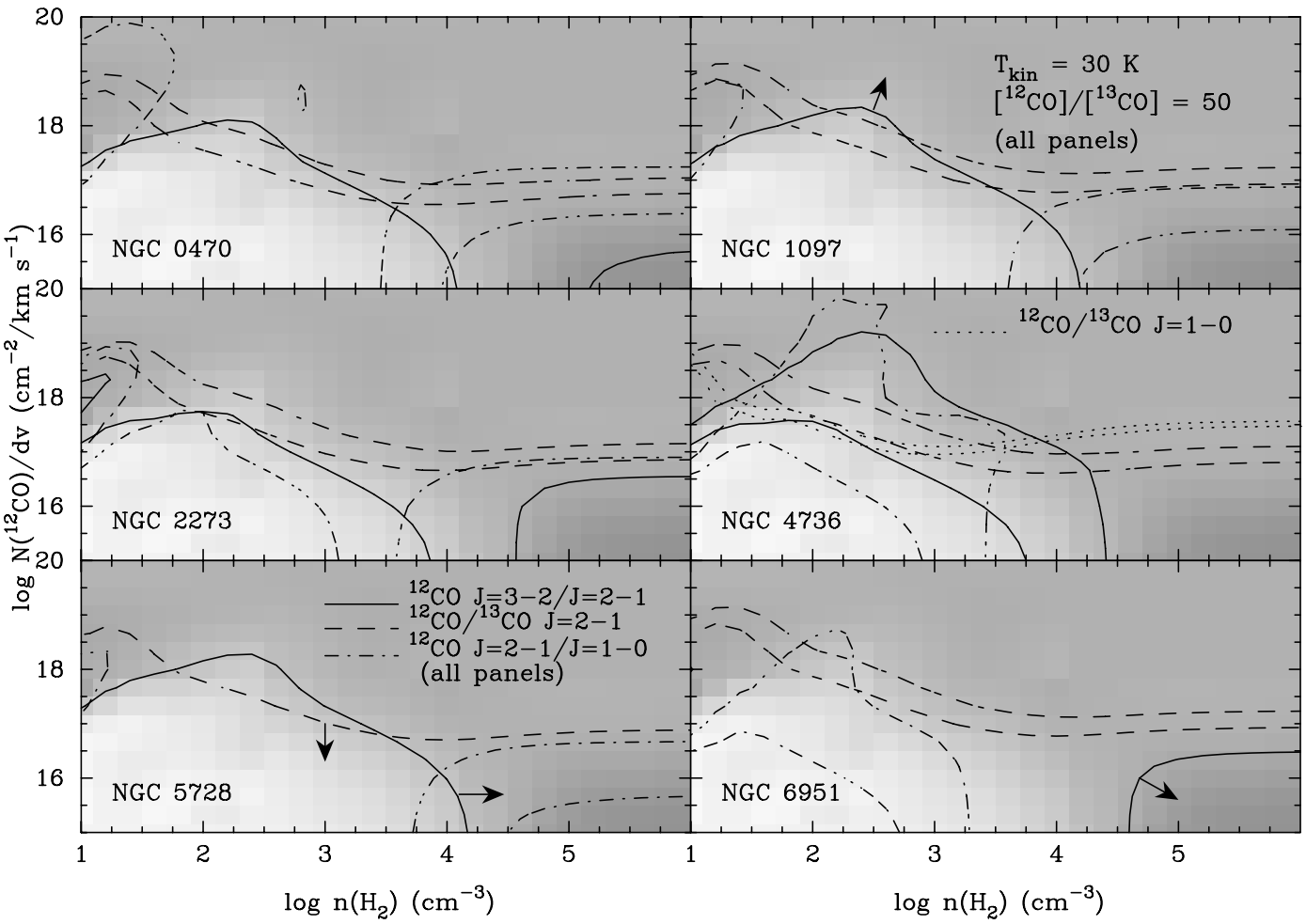

FIG. 4.—Plots of CO column density (per unit velocity) vs. H_2 density for a kinetic temperature of 30 K and a $^{12}CO/^{13}CO$ abundance ratio of 50. The contours represent the ±30% contours for the CO line ratios given in Table 4 and are indicated in the lower left panel. The underlying gray scale is the ^{12}CO $J = 3–2/J = 2–1$ line ratio. For NGC 4736 we have included the $^{12}CO/^{13}CO$ $J = 1–0$ ratio of Sage & Isbell (1991). Solutions appear as regions where all line ratios overlap. In the case where only one contour is visible on the plot, an arrow indicates the allowed regions.

density of CO, we must multiply by the velocity width of a typical molecular cloud in each galaxy. Unfortunately, the large beam of the JCMT covers many individual clouds in these distant galaxies in a single pointing, so the line width of individual clouds is difficult to determine. In the nearest galaxy in our sample (NGC 4736), our single-dish CO spectra shows emission features (e.g., $V_{LSR} = 225$ km s^{-1}; Fig. 1) with line widths of ~50 km s^{-1}. High-resolution ^{12}CO $J = 1–0$ maps of these galaxies indicate line widths of ~30–50 km s^{-1} (Kohno et al. 1999). Even these are still prone to the effects of galaxy rotation. For consistency, we assume that individual clouds in all galaxies have similar CO line widths of 10 km s^{-1}, similar to the Milky Way.

In the case of NGC 6951, our JCMT line ratios do not overlap in Figure 4. Thus, we cannot place strong constraints on the gas properties in the center of this galaxy. The values listed in Table 6 are determined using only the ^{12}CO $J = 3–2/J = 2–1$ line ratio and are not as firm as those determined for the other galaxies.

Adopting a line width of 10 km s^{-1} gives CO column densities of 10^{18} cm^{-3} for most of the galaxies in our sample. In order for star formation to occur, it is believed that the molecular gas must exceed some critical column density. This value is believed to be on the order of 10^{22} cm^{-3} (Solomon et al. 1987; Elmegreen 1989). Assuming a number density ratio of $n(CO)/n(H_2) = 10^{-4}$ (Genzel 1992), we find a column density of molecular hydrogen of 10^{22} cm^{-3}, which may explain why we see such a high level of nuclear activity in these galaxies.

3.3. *Overall Gas Properties from LTE and LVG*

The $J = 1$, $J = 2$, and $J = 3$ levels of CO lie at 5.5, 17, and 33 K above the ground state, respectively. In addition, in the optically thin limit where all CO emission escapes the cloud, the critical densities of H_2 needed to collisionally excite ^{12}CO at the same rate that it spontaneously decays are ~10^3, 10^4, and 10^5 cm^{-3} for the $J = 1–0$, α, and $J = 3–2$ transitions, respectively. So, fundamentally, higher ^{12}CO $J = 3–2/J = 2–1$ line ratios suggest that the molecular gas is warmer and/or denser.

In the simpler LTE approximation, we cannot accurately determine the density of the gas, but higher ^{12}CO $J = 3$–$2/J = 2$–1 line ratios suggest warmer gas in these galaxies. We do not have enough line ratios to place strong constraints on the gas properties using the LVG models, but, in general, higher ^{12}CO $J = 3$–$2/J = 2$–1 line ratios also indicate higher temperature (for a fixed density). Conversely, for a fixed temperature (which is feasible considering the similarities of the dust temperatures in these galaxies), the higher ^{12}CO $J = 3$–$2/J = 2$–1 line ratios indicate denser gas. So in either the LVG or LTE model, the higher ^{12}CO $J = 3$–$2/J = 2$–1 line ratio suggests warmer and/or denser gas.

The similarities in the ^{12}CO/^{13}CO $J = 2$–1 line ratios predict optical depths of $\sim$5 in all galaxies in both the LTE and LVG approximations (assuming Galactic values for the ^{12}CO^{13}CO abundance ratio of $\sim$50; Hawkins & Jura 1987; Langer & Penzias 1993). This similarity in optical depths makes the conclusions regarding temperature and density drawn from the ^{12}CO $J = 3$–$2/J = 2$–1 line ratio more convincing because we do not have to worry as much about variations in optical depth modifying the line ratio.

4. A CORRELATION OF CO LINE RATIOS WITH CENTRAL CO MORPHOLOGY

The existence of nuclear stellar bars in these galaxies strongly suggests that all of them contain an ILR (Shaw et al. 1993; Friedli et al. 1996). On the basis of existing data, we cannot accurately and uniformly determine the strength of the ILRs in these galaxies, so in this discussion we assume that our sample contains galaxies with similar ILR strengths. Table 2 shows that with the exception of NGC 4736 and NGC 5728, these galaxies share similar primary and secondary bar sizes and ellipticities, so it is not unreasonable to believe that the ILR strengths are similar in these galaxies. More detailed observations at high resolution of the dynamics of these galaxies are needed to confirm this and thus validate the following discussion.

The nuclear CO morphology of NGC 5728 resembles a clumpy structure that is not centered on the galactic center. It appears that it may be a lumpy circumnuclear ring that joins up with the southernmost dust lane (Petitpas & Wilson 2002). High-resolution CO maps of NGC 6951 show a "twin-peaked" structure that may be collections of molecular gas at the ILR (Kenney et al. 1992; Kohno et al. 1999). NGC 470 and NGC 2273 show CO distributions (Petitpas & Wilson 2002; Jogee 1998) that coincide with the nuclear stellar bars seen in the NIR images of Wozniak et al. (1995) and Mulchaey et al. (1997). The high-resolution CO maps of the inner 21″ of NGC 4736 show an elongated central peak that has been interpreted as a nuclear CO bar by Wong & Blitz (2000) and Sakamoto et al. (1999). We note that it is more centrally concentrated than the barlike features seen in CO in NGC 2273 and NGC 470.

There are currently no published high-resolution CO maps of NGC 3081 and NGC 1097 (likely because of their low declination). As such, we cannot include NGC 3081 in our comparison, but there are single-dish CO maps of NGC 1097 by Gerin, Combes, & Nakai (1988) that strongly suggest a circumnuclear ring of CO, with a radius of $\sim$8″. This is confirmed by the H I maps by Ondrechen, van der Hulst, & Hummel (1989), so we include this galaxy in our comparisons.

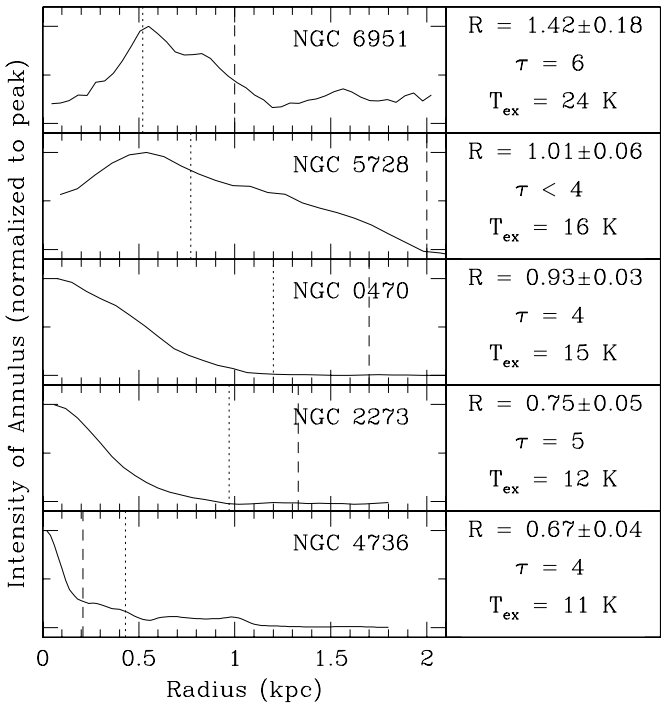

FIG. 5.—Radial profiles of the CO intensity compared to the ^{12}CO $J = 3$–$2/J = 2$–1 line ratio. The solid line is the azimuthally averaged CO distribution from high-resolution observations. The dotted line shows the location of the ILR as traced by the ends of the nuclear stellar bar and star-forming rings (when present; Friedli et al. 1996; Wozniak et al. 1995; Mulchaey et al. 1997). The dashed line represents the area covered by the JCMT primary beam. Also shown are the excitation temperatures and optical depths assuming LTE. They are arranged such that the galaxy with the highest line ratio is at the top, and the line ratio decreases as you move down. Note that the radial profiles become increasingly centrally concentrated as the line ratio decreases. Note that the bottom three galaxies are resolution-limited.

The data in Table 4 show evidence that galaxies containing elongated molecular barlike features in their central regions have lower ^{12}CO $J = 3$–$2/J = 2$–1 integrated intensity line ratios. This effect is emphasized in Figure 5, where we show the azimuthally averaged ^{12}CO $J = 1$–0 radial profile compared with the ^{12}CO $J = 3$–$2/J = 2$–1 line ratio and the properties determined in § 3.1. The profiles are ordered in decreasing value of the ^{12}CO $J = 3$–$2/J = 2$–1 line ratio. Clearly the degree of central concentration increases as you reach the cooler gas near the bottom of the figure. In the LVG approximation, the warmer and/or denser gas is at the top of the plot, and temperature and/or density decreases downward. We point out that there are resolution effects at work for the bottom three galaxies (NGC 4736, NGC 470, and NGC 2273). Since NGC 4736 is the closest galaxy in our sample, we are seeing it at the highest spatial resolution. Thus, in NGC 4736, our central peak appears much narrower than in NGC 2273 and NGC 470, but in reality, the width of each central peak is comparable to the resolution limit of the interferometer with which they were observed. Despite this, there is still an increasing tendency for the galaxies with lower ^{12}CO $J = 3$–$2/J = 2$–1 line ratios to have more centrally concentrated gas distributions, while the warmer (and possibly denser) gas appears to avoid the nucleus. Possible causes for this effect are discussed in § 5.

4.1. *Comparisons with Recent Models*

Previous models have indicated that in order to create and sustain nuclear bars and rings, there must be some form of viscous gas component that can dissipate energy (Combes & Gerin 1985; Athanassoula 1992; Friedli & Martinet 1993; Shaw et al. 1993). These models have reproduced many of the nuclear morphologies seen in single- and double-barred galaxies by varying the model's parameters such as bar pattern speed, main bar strength, ILR strength, etc. Some of these models have attempted to vary the gas viscosity parameter, which is usually assumed to be some numerical viscosity or some percentage of energy loss during cloud collision and kept constant for all trials. Our observational result is the first indication that gas properties may be related to the variety of molecular gas morphologies seen in the centers of double-barred galaxies.

Particularly relevant to this study are the studies of double-barred systems by Combes (1994) and Maciejewski et al. (2002). Combes (1994) studied the motions of molecular gas in a double-barred potential and found that in galaxies with more viscous gas, the nuclear bar becomes kinematically separate from the main bar (as predicted by Friedli & Martinet 1993), while in the less viscous model, the nuclear bar is actually rotating at the same pattern speed as the large-scale bar (as predicted by Shaw et al. 1993). In both cases, the molecular gas in the nucleus takes the form of a nuclear bar. We do not see these nuclear gas bars in all of the CO maps, so it is difficult to compare the observations with these models.

Maciejewski et al. (2002) modeled the gas response to a double-barred potential that could possibly be the result of purely stellar orbits. In this model, the gas distribution need not resemble the stellar distribution. In their models, they find that the double-barred potential is not capable of transporting molecular gas into the nucleus with the efficiency predicted by Shlosman et al. (1989). The gas still becomes trapped at the ILR, unless they increase the sound speed. In the simulations with higher sound speeds, the gas is capable of flowing all the way into the nucleus. It is interesting to note that our observations suggest that the galaxies with centrally concentrated gas distributions contain cooler, less dense gas, which could correspond to a higher sound speed. Thus, the gas in our double-barred galaxies may be flowing inward more efficiently in the galaxies with higher sound speeds as predicted by the models of Maciejewski et al. (2002), resulting in the more centrally concentrated CO profiles. However, until we can accurately measure the sound speed, this conclusion must remain rather speculative.

It seems more likely, however, that the variations in the gas distributions are affected strongly by star formation activity, which is not yet accounted for in these models. Future models of double-barred galaxies will need to include the effects of star formation in order to determine its effect on the flow of molecular gas into the centers of double-barred galaxies.

5. SPECULATIONS ON THE ORIGIN OF THE GAS PROFILE–GAS PROPERTY CORRELATION

5.1. *The Effect of Star Formation on Gas Properties*

We were unable to find estimates of the star formation rates (SFRs) of all these galaxies at high resolution using the same technique. In an attempt to keep the data sets used to compare the properties of the galaxies in our sample as uniform as possible, we have estimated the SFRs from the *IRAS* fluxes. While this may be the most accurate method for these dusty star-forming galaxy centers (Kennicutt 1998), the large beam of the *IRAS* satellite means that in all cases we are likely measuring the global SFR rather than the rates for the inner 21″ (the beam size of the JCMT). For now, we assume that the majority of the star formation in these galaxies is occurring in the central few kiloparsecs.

To estimate the SFR, we use the *IRAS* 60 and 100 μm fluxes to determine the infrared luminosity as described in Kohno et al. (1999). We then convert this luminosity to a star formation rate using the technique described in Hunter et al. (1986). To test the accuracy of our method, we compared the star formation rates for the entire galaxies determined from the *IRAS* fluxes to the direct measurement for the star formation rates using Hα data for the inner 45″ of a sample of different galaxies in Jogee (1998). We find that our star formation rates are generally $\sim$2–3 times higher than those determined by Jogee (1998), with somewhat larger discrepancies (up to 5 times higher) for the galaxies with low rates ($<1\ M_{\odot}\ \mathrm{yr}^{-1}$).

In Figure 6 we see that the ^{12}CO $J = 3$–$2/J = 2$–1 line ratio tends to be higher in the galaxies that show higher star formation rates. Given that we are likely overestimating the star formation rates of NGC 4736 and NGC 2273 to a higher degree than we are for NGC 5728 and NGC 6951 (for reasons described in the previous paragraph) it is likely that our result will hold when using a different technique to determine the star formation rates.

It is interesting to note that the variation in the gas properties with star formation activity discussed above, in conjunction with the correlation noted in § 4 (and shown in Fig. 5) indicates that the galaxies with higher star formation rates are depleted of molecular gas in their centers. One possible cause could be that the star formation and subsequent H II regions and supernovae deplete, photodissociate, and disrupt the clouds, leaving the galaxies with higher star

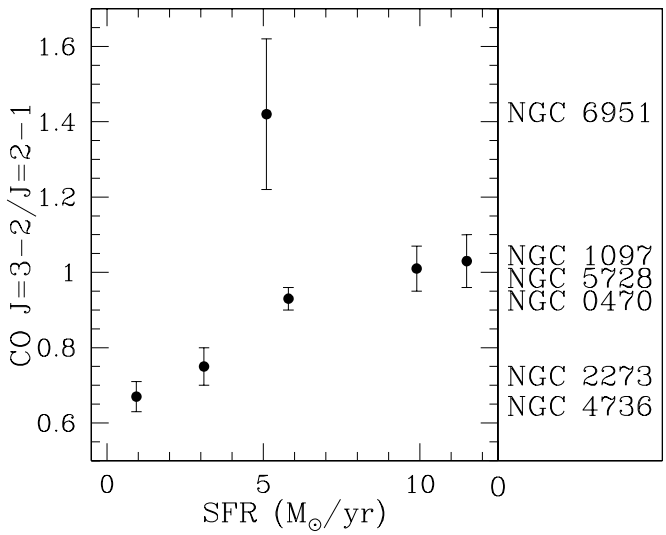

FIG. 6.—Comparison of (global) star formation rates to (nuclear) ^{12}CO $J = 3$–$2/J = 2$–1 line ratio. Since the optical depths are similar in each galaxy, the CO line ratio suggests that the gas is warmer and/or denser in the galaxies with higher star formation rates determined from *IRAS* fluxes. Higher resolution tracers of star formation activity and rates are needed to confirm this finding.

formation rates more gas-deficient in the nucleus, while heating and compressing the surrounding molecular gas. Without uniform, high-resolution observations of the star formation rates and locations, we cannot draw any firm conclusions from this analysis.

5.2. *The Effect of Gas Properties on Star Formation*

In the previous section we assumed that the dynamics in these galaxies were similar on the basis of the similarity of the NIR images. There are several unmeasured quantities that can change the central gas dynamics of these galaxies. One example is the bar pattern speed. Changing the pattern speed will change the strength of the ILR. We cannot rule out the possibility that the variation in gas distributions are caused by different strength ILRs. If this is the case, then the variations in star formation activity may be caused by the locations of the peaks in the gas distributions. For example, if the majority of gas is located at the ILR radius (a local stable point), it may be able to accumulate until it exceeds the critical density needed for star formation to occur (see, e.g., Elmegreen 1994 and references therein). Conversely, if the ILR is weak, the majority of the gas could accumulate in the central regions of the galaxy, where the local epicycle frequency (hence, critical density; Kennicutt 1989 and references therein) may be high enough to inhibit strong star formation in these galaxies. This may result in higher star formation rates in galaxies like NGC 6951 and NGC 1097, where the gas is concentrated near the ILR (Kohno et al. 1999; Gerin et al. 1988) than those galaxies with strong central concentration such as NGC 4736 (Wong & Blitz 2000).

A detailed study of a larger sample of galaxies combined with a more detailed analysis of the star formation histories and dynamics of these galaxies will help clarify this picture among double-barred galaxies.

6. SUMMARY

We have taken ^{12}CO $J = 3$–2, ^{13}CO $J = 3$–2, and ^{12}CO $J = 3$–2 spectra of the ILR regions of a sample of galaxies that show a double-barred nucleus in the near-infrared. We find that that ^{12}CO/^{13}CO $J = 2$–1 integrated intensity line ratio is uniform at the 2 σ level, while the ^{12}CO $J = 3$–2/$J = 2$–1 line ratio varies dramatically from galaxy to galaxy.

We find that the CO $J = 3$–2/$J = 2$–1 line ratio is higher in galaxies with noncentralized CO distributions and lower in galaxies that contain centralized concentrations. The uniform ^{12}CO/^{13}CO $J = 2$–1 line ratios suggest that the molecular gas is marginally optically thick, with $\tau \sim 5$ in all galaxies. The similarity in optical depths suggests that the variation in the ^{12}CO $J = 3$–2/$J = 2$–1 line ratio is indicating real variations in the gas properties. This result suggests that the molecular gas is cooler and/or less dense in galaxies that contain central concentrations and warmer and/or denser in galaxies with less centrally concentrated CO distributions.

There is some evidence that the star formation rates are higher in the galaxies that have warmer/denser, noncentrally concentrated gas distributions. This result suggests that the star formation activity may be depleting the central gas while heating and compressing the surrounding molecular gas resulting the the observed variety of gas distributions and physical conditions.

It is also possible that bar dynamics alone is responsible for modifying the gas distributions, densities, and star formation rates. In this scenario the enhanced star formation is the result of stronger ILRs allowing molecular gas to accumulate to high (supercritical) densities near the ILR radius. A more detailed study of the star formation activity and internal dynamics of these galaxies at higher resolution is needed to disentangle these.

It seems evident based on these observations that future models of double-barred galaxies will need to include star formation in order to disentangle the effects of dynamics and star formation activity.

This research has been supported by a research grant to C. D. W. from NSERC (Canada). G. R. P. is supported by NSF grant AST 99-81289 and by the State of Maryland via support of the Laboratory for Millimeter-Wave Astronomy. This research has made use of the NASA/IPAC Extragalactic Database (NED), which is operated by the Jet Propulsion Laboratory, California Institute of Technology, under contract with the National Aeronautics and Space Administration. We wish to thank S. Jogee for providing the CO data for NGC 6951 and NGC 470 from her Ph.D. thesis and T. Wong for providing the data for NGC 4736 so that we could calculate the radial profiles. We also wish to thank the referee Eric Emsellem for detailed comments that greatly improved the clarity and quality of this paper.

REFERENCES

Aalto, S., Booth, R. S., Black, J. H., & Johansson, L. E. B. 1995, A&A, 300, 369
Athanassoula, E. 1992, MNRAS, 259, 345
Combes, F. 1994, in Mass Transfer-induced Activity in Galaxies, ed. I. Shlosman (Cambridge: Cambridge Univ. Press), 170
Combes, F., & Gerin, M. 1985, A&A, 150, 327
Devereux, N. A., & Young, J. S. 1990, ApJ, 359, 42
Elmegreen, B. G. 1989, ApJ, 338, 178
———. 1994, ApJ, 425, L73
Friedli, D., & Martinet, L. 1993, A&A, 277, 27
Friedli, D., Wozniak, H., Rieke, M., Martinet, L., & Bratschi, P. 1996, A&AS, 118, 461
Genzel, R. 1992, in The Galactic Interstellar Medium, ed. D. Pfenniger & P. Bartholdi (Berlin: Springer), p. 275
Gerin, M., Casoli, F., & Combes, F. 1991, A&A, 251, 32
Gerin, M., Combes, F., & Nakai, N. 1988, A&A, 203, 44
Hawkins, I., & Jura, M. 1987, ApJ, 317, 926
Hunter, D. A., Gillett, F. C., Gallagher, J. S., Rice, W. L., & Low, F. J. 1986, ApJ, 303, 171
Jogee, S. 1998, Ph.D. thesis, Yale Univ.
Jogee, S., Kenney, J. D. P., & Smith, B. J. 1999, ApJ, 526, 665
Jungwiert, B., Combes, F., & Axon, D. J. 1997, A&AS, 125, 479
Kenney, J. D. P., Wilson, C. D., Scoville, N. Z., Devereux, N. A., & Young, J. S. 1992, ApJ, 395, L79
Kennicutt, R. C. 1998, ARA&A, 36, 189
———. 1989, ApJ, 344, 685
Kohno, K., Kawabe, R., & Vila-Vilaró, B. 1999, ApJ, 511, 157
Kruegel, E., Chini, R., & Steppe, H. 1990, A&A, 229, 17
Kutner, M. L., & Ulich, B. L. 1981, ApJ, 250, 341
Langer, W. D., & Penzias, A. A. 1993, ApJ, 408, 539
Maciejewski, W., Teuben, P. J., Sparke, L. S., & Stone, J. M. 2002, MNRAS, 329, 502
Moellenhoff, C., Matthias, M., & Gerhard, O. E. 1995, A&A, 301, 359
Moshir, M. E. A., et al. 1990, *IRAS* Faint Source Catalogue, Version 2.0 (Pasadena: IPAC)
Mulchaey, J. S., Regan, M. W., & Kundu, A. 1997, ApJS, 110, 299
Ondrechen, M. P., van der Hulst, J. M., & Hummel, E. 1989, ApJ, 342, 39
Petitpas, G. R., & Wilson, C. D. 2000, ApJ, 538, L117
———. 2002, ApJ, 575, 814
Phillips, M. M., Charles, P. A., & Baldwin, J. A. 1983, ApJ, 266, 485

Sage, L. J., & Isbell, D. W. 1991, A&A, 247, 320
Sakamoto, K., Okumura, S. K., Ishizuki, S., & Scoville, N. Z. 1999, ApJ, 525, 691
Scheffler, H., & Elsaesser, H. 1987, Physics of the Galaxy and Interstellar Matter (Berlin: Springer)
Shaw, M. A., Combes, F., Axon, D. J., & Wright, G. S. 1993, A&A, 273, 31
Shioya, Y., Tosaki, T., Ohyama, Y., Murayama, T., Yamada, T., Ishizuki, S., & Taniguchi, Y. 1998, PASJ, 50, 317
Shlosman, I., Frank, J., & Begelman, M. C. 1989, Nature, 338, 45
Sofue, Y., Wakamatsu, K., Taniguchi, Y., & Nakai, N. 1993, PASJ, 45, 43
Soifer, B. T., Boehmer, L., Neugebauer, G., & Sanders, D. B. 1989, AJ, 98, 766
Solomon, P. M., Rivolo, A. R., Barrett, J., & Yahil, A. 1987, ApJ, 319, 730
Stutzki, J., & Güsten, R. 1990, ApJ, 356, 513
Tilanus, R. P. J., Tacconi, L. J., Sutton, E. C., Zhou, S., Sanders, D. B., Wynn-Williams, C. G., Lo, K. Y., & Stephens, S. A. 1991, ApJ, 376, 500
Vila-Vilaró, B., Taniguchi, Y., & Nakai, N. 1998, AJ, 116, 1553
Wong, T., & Blitz, L. 2000, ApJ, 540, 771
Wozniak, H., Friedli, D., Martinet, L., Martin, P., & Bratschi, P. 1995, A&AS, 111, 115